Differentiation 148 (2026) 100944

Contents lists available at ScienceDirect

Differentiation

journal homepage: www.elsevier.com/locate/diff

Low and high osteogenic potential of periodontal ligament-derived mesenchymal stem cells correlates with RUNX2, SP7, EZH2 and KDM6B expression

D.C. Andia [a,*], L.F. Oliveira [a], G.S. Feltran [b], A.A.S. Gonçalves [c], W.F. Zambuzzi [b], R.A. da Silva [c]

[a] Dental Research Division, School of Dentistry, Health Science Institute, Paulista University - UNIP, São Paulo, Brazil
[b] Department of Chemistry and Biochemistry, Lab. of Bioassays and Cellular Dynamics, Institute of Biosciences, UNESP – São Paulo State University, Botucatu, Brazil
[c] CEEpiRG, Program in Environmental and Experimental Pathology, Paulista University – UNIP, São Paulo, Brazil

ARTICLE INFO

Keywords:
Osteogenesis
Epigenomics
Chromatin
Histones
Stem cells
Transcription factor

ABSTRACT

Periodontal ligament-derived mesenchymal stem cells (PDLCs) possess selfrenewal and multilineage differentiation capacities, supporting their application in regenerative therapies. However, PDLCs are regulated by epigenetic mechanisms that influence chromatin accessibility and gene expression, and may exhibit distinct phenotypes under osteogenic conditions. This study aimed to investigate whether differences in osteogenic potential of PDLCs (h-PDLCs and l-PDLCs, high and low, respectively) correlate with the expression of key transcription factors and epigenetic regulators. We performed qPCR for mRNA expression analysis, immunofluorescence, and Western blotting for protein levels, as well as chromatin immunoprecipitation followed by qRT-PCR to investigate H3K27me3 enrichment at the *RUNX2* and *SP7* promoter regions in PDLCs cultured under basal conditions (DMEM, T0) and after 3 and 10 days of osteogenic induction (T3 and T10). At baseline, h-PDLCs and l-PDLCs exhibited distinct transcriptional and protein profiles. During osteogenic stimulation, *EZH2* expression significantly increased in l-PDLCs but decreased in h-PDLCs ($p < 0.001$), while *KDM6B* expression decreased in l-PDLCs and increased in hPDLCs ($p < 0.0001$). Analysis of *RUNX2*, *RUNX2p57*, and *SP7* revealed dynamic transcriptional modulation: *RUNX2p57* and *SP7* were downregulated in l-PDLCs ($p < 0,001$), whereas *RUNX2* was upregulated in h-PDLCs (T3 and T10, $p < 0,0001$). Furthermore, l-PDLCs exhibited greater accumulation of the repressive histone mark H3K27me3, with significant enrichment at the *RUNX2* and *SP7* promoter regions compared to h-PDLCs during osteogenic induction ($p < 0.05$). Together, these findings demonstrate that low and high osteogenic potential of PDLCs correlate with coordinated differences in the expression of the transcription factors RUNX2 and SP7 and the epigenetic regulators EZH2 and KDM6B, as well as with H3K27me3 enrichment patterns.

1. Introduction

The oral cavity is a valuable source of mesenchymal stem cells (MSCs), identified in tissues such as gingiva, dental pulp, and periodontal ligament (Hargreaves et al., 2013). Among these, periodontal ligament-derived mesenchymal stem cells (PDLCs) exhibit exceptional self-renewal and multilineage differentiation potential, making them promising candidates for bone and dental tissue engineering (Cabaña-Muñoz et al., 2023). PDLCs display higher proliferative rates than adipose-derived stem cells and possess angiogenic properties, further supporting their potential in regenerative applications (Yeasmin et al., 2014; Liu et al., 2022).

For clinical purposes, PDLCs must differentiate into osteoblasts capable of mineral deposition. However, their osteogenic commitment varies among individuals (Assis et al., 2021; Assis et al., 2021; Ferreira et al., 2022; Adolpho et al., 2022; Assis et al., 2022; Ferreira et al., 2023; Ferreira et al., 2024). Under osteogenic conditions, PDLCs can adopt phenotypes with either high (h-PDLCs) or low (l-PDLCs) mineralization

* Corresponding author. Dental Research Division, School of Dentistry, Health Science Institute, PaulistaUniversity, Dr. Bacelar St, 1212, São Paulo, SP, 04026-002, Brazil.
E-mail address: denise.andia@docente.unip.br (D.C. Andia).

https://doi.org/10.1016/j.diff.2026.100944
Received 15 September 2025; Received in revised form 27 January 2026; Accepted 2 February 2026
Available online 5 February 2026

potential. Previous studies have shown that l-PDLCs exhibit hypermethylation of osteogenic genes, impairing their differentiation capacity and delaying mineralization (Assis et al., 2021; Assis et al., 2022; Ferreira et al., 2022).

RUNX Family Transcription Factor 2 (RUNX2) and Sp7 Transcription Factor (SP7) are widely recognized as key regulators of osteoblast differentiation. The RUNX2/p57 isoform plays a pivotal role in osteoblastic phenotype development and is tightly regulated by both repressive and activating epigenetic mechanisms (Ducy et al., 1997; Meyer et al., 2014; Tai et al., 2014; Wu et al., 2014; Rojas et al., 2015; Aguilar et al., 2016). In murine models, deletion of either Runx2 or Sp7 abolishes bone formation, confirming their essential role in skeletal development and their relevance to human bone disorders (Mundlos et al., 1997; Lapunzina et al., 2010). Moreover, Sp7 deficiency disrupts differentiation of Runx2-expressing precursors (Zhou et al., 2010).

The osteogenic potential of MSCs is modulated by epigenetic mechanisms affecting chromatin accessibility, such as histone methylation and acetylation. Polycomb Repressive Complexes (PRC1 and PRC2) mediate chromatin silencing, with Enhancer of Zeste Homolog 2 (EZH2), the catalytic subunit of PRC2, catalyzing H3K27me3, a repressive histone mark associated with transcriptional silencing of osteogenic genes (Yu et al., 2008; Voigt et al., 2013). In contrast, lysine demethylase 6 B (KDM6B) removes H3K27me3, promoting lineage-specific gene activation and differentiation (Yeasmin et al., 2014). KDM6B is a recognized regulator of osteogenic and odontogenic differentiation in MSCs (Yeasmin et al., 2014).

Pharmacological inhibition of histone methylation has been shown to restore RUNX2 and SP7 expression, increase alkaline phosphatase (ALPL) activity, and enhance mineral deposition (Gopinathan et al., 2013), suggesting that the osteogenic profile of periodontal progenitors is associated with epigenetic regulation. Epigenomic and transcriptomic analyses comparing h-PDLCs and l-PDLCs identified EZH2 and KDM6B as key regulators influencing chromatin accessibility and osteogenesis-related gene expression (Assis et al., 2022).

Understanding these regulatory associations is important for elucidating features of osteogenic commitment in PDLCs and may contribute to novel strategies for regenerative, cell-based therapies. This study investigates the epigenetic regulation of osteogenic differentiation in PDLCs with distinct commitment, focusing on the association between EZH2, KDM6B and H3K27me3 profiles and *RUNX2/SP7* transcriptional patterns in PDLCs with distinct osteogenic commitment *in vitro*.

2. Material and methods

PDLCs were collected from extracted third molars from two subjects aged between 20 and 22 years, after signing an informed consent (CAAE55588816.4.0000.5418). The clinical data of tissue donor, isolation, culture of PDLCs, population doubling times, the characterization of their ability to osteogenic differentiation, epigenetic and transcriptomic profiles are detailed in our previous publications (Assis et al. 2021, 2022; Ferreira et al. 2022, 2023, 2024). PDLCs with low (l-PDLCs) and high (h-PDLCs) osteogenic profiles were cultured and analyzed at T0 - baseline (DMEM) and in osteogenic induction (OM) for 3 days (T3) and 10 days (T10). Cells at passages P6 – P8 were used with three biological replicates for each experiment, except when stated otherwise.

2.1. In vitro osteoblast-differentiation model

L-PDLCs and h-PDLCs (25×10^4 cells) were seeded into 6-well plates in DMEM medium, containing 10% FBS and 1% Pen/Strep. The *in vitro* osteogenic induction was performed with osteogenic medium (OM) (ascorbic acid 50 μg/mL, β-glycerolphosphate 10 mM, dexamethasone 10 nM), supplemented with 10% FBS and 1% Pen/Strep for 3 and 10 days (T3 and T10 groups, respectively). The control group (DMEM, baseline, T0) was collected on the first day, immediately before the onset of osteogenic induction.

2.2. RNA isolation, cDNA synthesis, and quantitative real time PCR (qRT-PCR)

Total RNA was extracted by TRIzol:chloroform method (Invitrogen, Thermo Fisher Scientific Inc., IL, USA) and 2 μg of total RNA was used for cDNA synthesis with Superscript II (Invitrogen, Thermo Fisher Scientific Inc., IL, USA), according to manufacturer's instructions. qPCR was carried out in a total of 10 μL, containing 5 μL of real-time PCR master mix (PowerUp™ SYBR™ Green Master Mix 2x; Applied Biosystems, CA, USA), 1 μL of specific primers (10 μM), 30 ng of cDNA, and nuclease free H_2O in a real-time PCR master mix and thermal cycler (LightCycler 96 Instrument, Roche, USA). The results of three biological replicates are presented as relative amounts of the target gene using *ACTB* or *18S* as inner reference genes. The primers sequences and PCR conditions are shown in Appendix Table 1.

2.3. Immunofluorescence

The cells were incubated with primary antibody for H3k27me3 (Cell Signaling, Danvers, MA, USA) and stained with Alexa Fluor 594 anti-rabbit or mouse IgG (Invitrogen/Molecular Probes, Waltham, MA), followed by staining with Alexa Fluor 488-labelled phalloidin probe (Invitrogen/Molecular Probes, Waltham, MA), following the manufacturer's instructions and previous publication (da Silva RA et al., 2019). The coverslips were mounted on glass slides using Fluoroshield with 4′, 6-Diamidine-2′-phenylindole dihydrochloride (DAPI) (Sigma, St. Louis, MO, USA) and then visualized under an inverted laser scanning confocal microscope (Leica TCS SP5).

2.4. Western blotting analysis

The protein extracts were obtained using a RIPA lysis buffer (Sigma Aldrich) supplemented with protease inhibitors (Sigma Aldrich, Darmstadt, Germany) and the concentrations were determined using the Lowry protein assay (da Silva RA et al., 2019). Equal amounts of protein (50 μg) were loaded onto SDS-PAGE and blotted onto polyvinylidene difluoride membranes (Millipore, Bedford, MA, USA) that were blocked and incubated overnight at 4 °C with the primary antibody for TriMethyl-Histone H3 (Cell Signaling, MA, USA) and Histone H3 (Cell Signaling, MA, USA) and then with appropriate HRP-linked secondary antibodies in blocking buffer for 1 h. Immunoreactive bands were detected with an enhanced chemiluminescence kit (BIORAD, California, USA). Densitometric analysis of immunoblots were measured using the ImageJ Software (U. S. National Institutes of Health, Bethesda, MD, USA) normalized to the protein ratio of controls, which were normalized by 1, with H3 as loading control.

2.5. Chromatin immunoprecipitation (ChIP) and qRT-PCR analysis

ChIP analysis was performed as previously described [28], with some modifications as described below, according to groups and periods of time explained before in l-PDLCs e hPDLCs. Briefly, 1×10^6 cells plated and grown on 150 mm dishes were crosslinked with 1.1% formaldehyde for 10 min at 37 °C and the reaction quenched with 2,5 M glycine in DPBS for 10 min. The cells were then washed two times in cold DPBS, harvested, pooled, flash frozen, and stored at −80 °C. For each immunoprecipitation, 1×10^6 cells were first incubated in lysis buffer 1 (50 mM HEPES-KOH, pH 7.5, 140 mM NaCl, 1 mM EDTA, 10% glycerol, 0.5% NP40, 0.25% Triton X-100, 1x protease inhibitors) followed by resuspension in lysis buffer 2.

(10 mM Tris-HCl, pH 8.0, 100 mM NaCl, 1 mM EDTA, 0.5 mM EGTA, 0.1% Na-deoxycholate, 0.5% N-lauroylsarcosine, 1 × protease inhibitors). The chromatin was then sheared to a size up to 200 bp using a cup horn sonicator (Fischer Scientific, Waltham, MA, USA) and clarified

at 12,000 rpm for 10 min. An input fraction corresponding to 5% of the starting material was kept aside for ChIP normalization. Immunoprecipitation reactions were performed by incubating equal amounts of 200 μg of sheared chromatin with 100 μL of Dynabeads (Life Technologies, Carlsbad, CA, USA) prebound to 10 μg of antibody against the histone modification H3K27me3, histone H3K27 and IgG (Cell Signaling, Danvers, MA, USA). After overnight incubation at 4 °C, beads were washed 5 times with 1X RIPA buffer (50 mM HEPES-KOH, pH 7.5; 500 mM LiCl; 1 mM EDTA; 1.0% NP40; 0.7% Na-deoxycholate) and once with 1X TE (10 mM Tris-HCl pH 8.0; 1 mM EDTA pH 8.0). Elution of protein-DNA

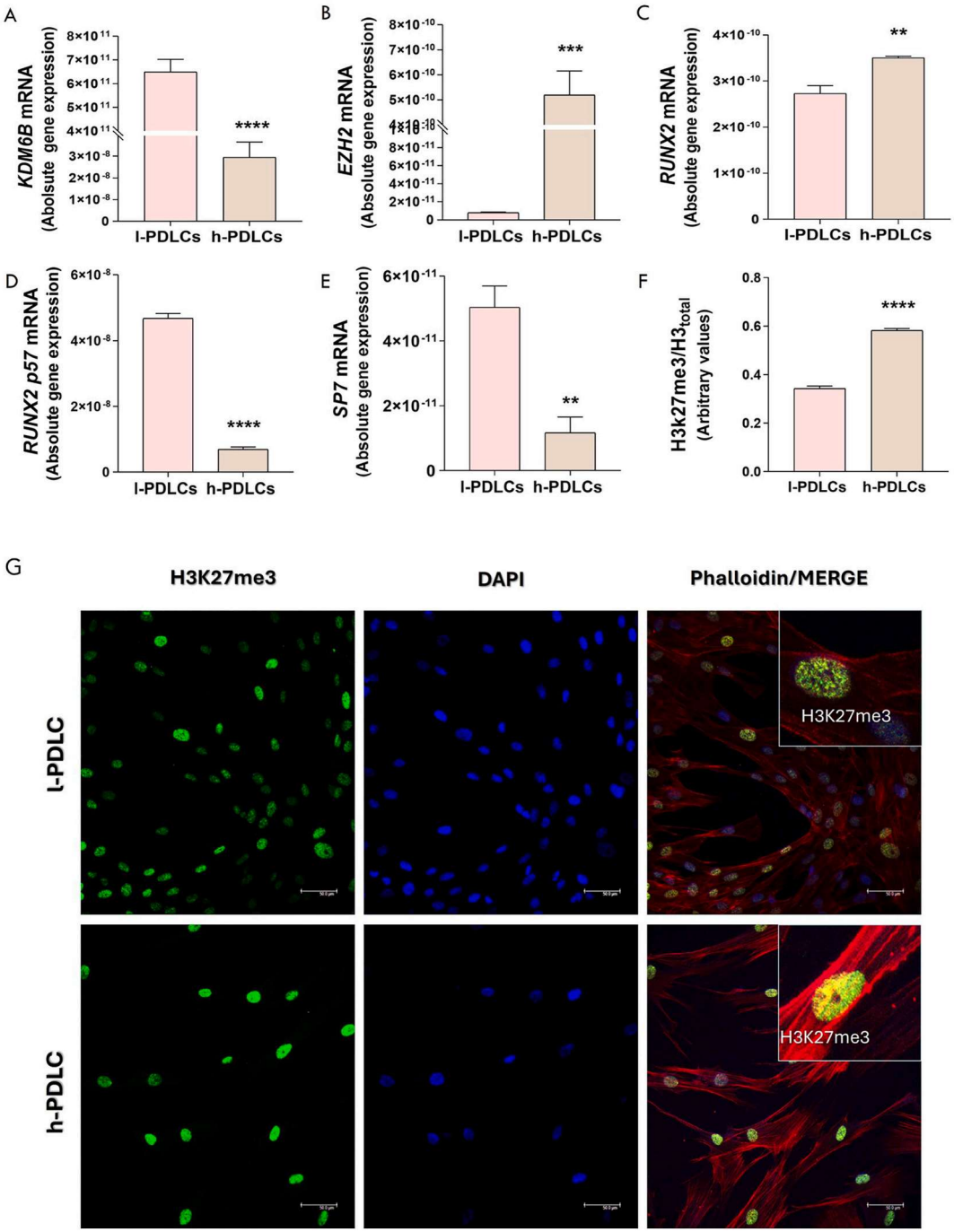

Fig. 1. Basal characterization of the epigenetic mark H3K27me3, the epigenetic enzymes associated with H3K27me3 levels and key osteogenic genes. qPCR results comparing transcript levels of *EZH2*, *KDM6B*, *RUNX2*, *RUNX2p57* and *SP7* (A-E). (F) WB results of H3K27me3/H3 in h-PDLCs and l-PDLCs. Three biological repeats were obtained for each group, each analyzed in technical triplicates. The relative gene expression levels were determined by using the cycle threshold (Ct) method, and correspond to mRNA levels ratio normalized to *ACTIN-B* levels. Statistical diferences were performed by T Test (**p ≤ 0.01; ***p ≤ 0.001; ****p ≤ 0.0001). Values are displayed as mean ± SD. (G) lPDLCs and h-PDLCs were subject to immunostaining analysis and the data show an increase in the immunostaining of H3K27me3 in the h-PDLCs. Nuclei were labelled with DAPI (blue) and cell membrane was labelled with falloindin conjugated with 633. Magnification ×40 (bars = 50 m). qPCR, quantitative polymerase chain reaction; PDLCs, periodontal ligament cells; h-PDLCs, high osteogenic potential; l-PDLCs, low osteogenic potential; *EZH2*, Enhancer of Zeste 2 Polycomb Repressive Complex 2; *KDM6B*, Lysine Demethylase 6 B; *RUNX2*, Runt-Related Transcription Factor 2; *RUNX2 p57*, bone-specific isoform of Runt-Related Transcription Factor 2; *SP7*, Sp7 Transcription Factor; H3K27me3, tri-methylation of lysine 27 on histone H3; H3, Histone 3.

complexes was carried out by incubating beads in elution buffer (50 mM Tris-HCl, pH 8.0; 10 mM EDTA; 1.0% SDS) followed by crosslink reversal at 65 °C overnight. DNA purification was carried out using DNA Clean & Concentrator kit (Zymo Research, Irvine, CA, USA), following manufacturer's guidelines. Real-time quantitative polymerase chain reaction (PCR) was performed with SYBR green Master Mix (Life Technologies, Carlsbad, CA, USA) on a LightCycler 96 Instrument (Roche, Basel, Switzerland), using specific primer pairs against promoter regions of *RUNX2* and *SP7* [28] (Table 1). Amplification data for each primer pair were normalized to input chromatin of H3K27, and histone modification enrichment data are presented after subtracting the values of corresponding negative controls (beads alone). Graphed data are from two independent ChIP reactions, in technical triplicates at PCR run, performed for each condition and experimental period in each cell type.

2.6. Statistical analysis

All data were first evaluated for normality and homogeneity of variance. Gene expression levels of *EZH2*, *KDM6B*, *RUNX2*, *RUNX2p57*, *SP7* and H3K27me3 protein at basal conditions were analyzed using an unpaired *t*-test. For comparisons across basal and osteogenic conditions, gene expression levels of *EZH2*, *KDM6B*, *RUNX2*, *RUNX2p57*, *SP7*, and H3K27me3 protein were assessed using one-way ANOVA followed by Tukey's post hoc test. Histone H3K27me3 enrichment data were analyzed by two-way ANOVA followed by Tukey's post hoc test. All statistical analyses were performed using GraphPad Prism version 10.2.3 (GraphPad Software, San Diego, CA, USA), and results were considered statistically significant at $p \leq 0.05$.

3. Results

3.1. At basal conditions, l-PDLCs and h-PDLCs possesses distinct transcriptional, protein and epigenetic landscapes associated with osteogenic differentiation

The transcript levels of *KDM6B* (Fig. 1A) were significantly higher in l-PDLCs compared to h-PDLCs ($p \leq 0.0001$), consistent with a chromatin profile commonly associated with a more active chromatin state in l-PDLCs. In contrast, *EZH2* (Fig. 1B) gene expression was significantly elevated in h-PDLCs, reflecting a more repressive epigenetic profile at basal condition. Regarding *RUNX2* (Fig. 1C) we have observed a significantly higher expression in h-PDLCs than in l-PDLCs ($p \leq 0.01$). On the contrary, *RUNX2p57* (Fig. 1D) and *SP7* (Fig. 1E) exhibited significantly higher expression levels in l-PDLCs than in h-PDLCs. At the protein level, the H3K27me3/H3 ratio (Fig. 1F) was higher in h-PDLCs, consistent with their increased *EZH2* expression, which is associated with a more repressive chromatin state. These findings indicate that, at the basal condition, l-PDLCs and h-PDLCs possesses distinct transcriptional and epigenetic landscapes associated with osteogenic differentiation.

Fig. 1G shows an increase in the immunostaining of H3K27me3 in the h-PDLCs, corroborating with the gene expression scenario observed in the *KDM6B* and *EZH2* transcript levels (Fig. 1A and B).

3.2. EZH2 and KDM6B are dynamically regulated during osteogenic differentiation in PDLCs

For l-PDLCs, at basal levels (T0), *EZH2* gene expression was relatively low, however, following 3 days of osteogenic stimulation, there was a significant increase ($p \leq 0.001$) in its mRNA levels (x T0). In the sequence, at 10 days of stimulation, the expression level showed a significant decrease ($p \leq 0.01$) compared to T3 (Fig. 2A). On the other hand, the h-PDLCs showed basal transcript levels similar to T3, with a significant decrease at T10 ($p \leq 0.001$) (Fig. 2C). The *KDM6B* gene expression in l-PDLCs was higher in T0, with a significant decrease at T3 and T10 (Fig. 2B). While the gene expression of *KDM6B* decreases over time in l-PDLCs, the opposite pattern occurs in h-PDLCs. At T3, a significant upregulation ($p \leq 0.01$) was detected and at T10, the expression increased even more compared to T3 ($p \leq 0.001$) and T0 ($p \leq 0.0001$) (Fig. 2D).

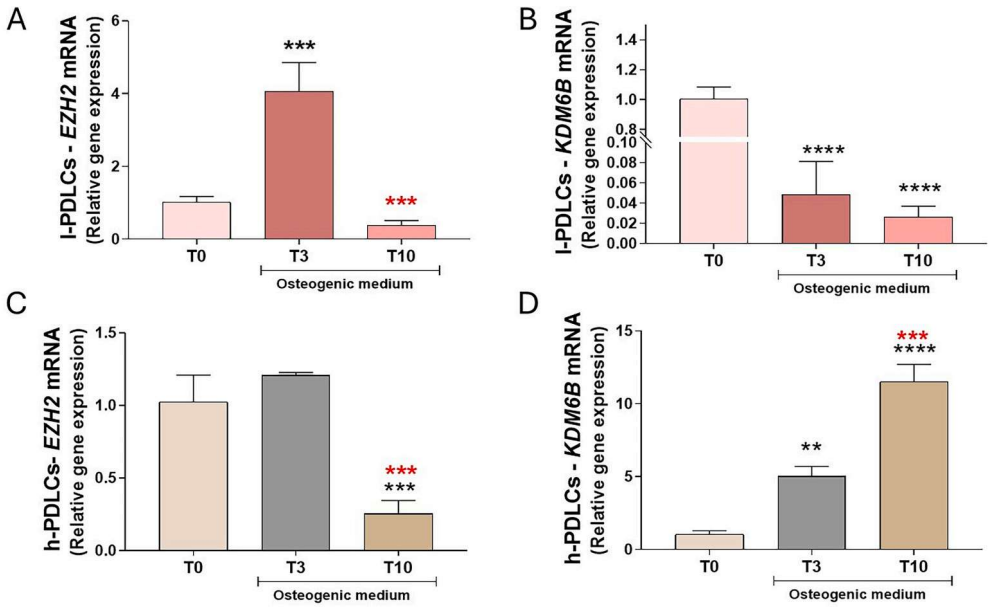

Fig. 2. Transcriptional profile of the epigenetic enzymes *EZH2* and *KDM6B* in PDLCs with distinct osteogenic phenotype during osteogenic induction. Graphics show the qPCR results of *EZH2* (A, C) and *KDM6B* (B, D) in l-PDLCs and h-PDLCs at basal levels (T0) and after 3 and 10 days of osteogenic stimulus (T3 and T10). The relative gene expression levels were determined by using the cycle threshold (Ct) method, and correspond to mRNA levels ratio normalized to *ACTIN-B* levels. The results are represented as mean ± SD of three independent experiments. Statistical diferences were performed by ANOVA one way followed by Tukey test. **$p \leq 0.01$, ***$p \leq 0.001$ and ****$p \leq 0.0001$ compared to T0; ***$p \leq 0.001$ compared to T3. h-PDLCs, high osteogenic potential; l-PDLCs, low osteogenic potential.

3.3. Dynamic transcriptional regulation of key osteogenic genes during osteogenic stimulus

For l-PDLCs, at baseline (T0), all three genes exhibited high expression levels. Upon 3 days of osteogenic stimulation, a significant increase in *RUNX2* expression was observed ($p \leq 0.05$), followed by a reduction at 10 days ($p \leq 0.0001$ x T3), consistent with patterns typically associated with early osteogenic commitment. *RUNX2p57* and *SP7* gene expressions showed an opposite trend, with significantly reduced expression at T3 and T10 compared to T0, suggesting both gene transcripts might be downregulated during differentiation in these cells (Fig. 3B and C). These findings highlight dynamic transcriptional patterns of key osteogenic genes that correlate with differences in osteogenic potential between PDLC populations, where *RUNX2* is transiently upregulated during early differentiation, while *RUNX2p57* and *SP7* show progressive downregulation in l-PDLCs.

In h-PDLCs, *RUNX2* expression increased at T3 and remained elevated at T10, with significant differences compared to T0 ($p \leq 0.0001$) (Fig. 3D). Conversely, *RUNX2p57* and *SP7* showed significant downregulations at T10 compared to T3 ($p \leq 0.0001$), indicating an early activation but later downregulation as osteogenic differentiation progresses (Fig. 3E and F).

3.4. l-PDLCs exhibit a more pronounced accumulation of H3K27me3

In l-PDLCs (Fig. 4A), H3K27me3/H3 levels showed a progressive and significant increase over time, with expression at T10 being significantly higher than at T0 ($p \leq 0.0001$), indicating enhanced chromatin repression during osteogenic induction. In contrast, h-PDLCs (Fig. 4B) exhibited a more moderate increase in H3K27me3/H3 levels across time points. When comparing both populations, l-PDLCs consistently exhibited higher H3K27me3/H3 levels, particularly at T10, reaching almost 4 times more than T0, suggesting a more repressive epigenetic landscape associated with osteogenic differentiation in these cells. These findings showed l-PDLCs presented a more pronounced accumulation of the repressive histone mark H3K27me3, potentially reflecting their lower osteogenic potential compared to h-PDLCs.

3.5. H3K27me3 is differentially enriched at RUNX2 and SP7 promoters in l-PDLCs and h-PDLCs during osteogenic induction

To investigate the enrichment of the repressive mark H3K27me3, specific sites within the promoter regions of the osteogenic markers *RUNX2* and *SP7* were strategically selected for analysis. The results presented in Fig. 5(A–C) indicate the H3K27me3 enrichment at the *RUNX2* and *SP7* promoters differs between l-PDLCs and h-PDLCs over the osteogenic induction. In l-PDLCs, although there was a tendency of increased levels at T3, this increase was not statistically significant comparing to T0 or T10; on the other hand, it was significant compared to h-PDLCs (T10) ($p < 0.05$); in contrast, in h-PDLCs, H3K27me3 enrichment is significantly decreased at T10 x T0 ($p < 0.05$) (Fig. 5A). The higher levels of H3K27me3 enrichment in l-PDLCs (T3) x h-PDLCs (T10) and the decrease in the H3K27me3 enrichment over time in h-PDLCs, suggest a less repressive chromatin state at the *RUNX2* promoter in h-PDLCs. Similarly, Fig. 5B shows H3K27me3 enrichment at the *SP7* promoter of h-PDLCs follows a comparable pattern to *RUNX2*, decreasing its levels over the osteogenic induction period, being significant lower at T10. In another specific site within the *SP7* promoter region (Fig. 5C), no statistically significant differences were observed across time points or between cell populations, suggesting a finely tuned epigenetic regulation not only at the gene level but also at distinct regions within the same gene promoter. These findings highlight a differential epigenetic regulation of *RUNX2* and *SP7* between these two cell populations, which, when associated with other regulatory epigenetic mechanisms, may reflect epigenetic features associated with differences in osteogenic potential.

4. Discussion

The molecular mechanisms underlying the heterogeneity of the osteogenic commitment of PDLCs remain poorly understood. Our group has investigated epigenetic regulatory pathways modulating the

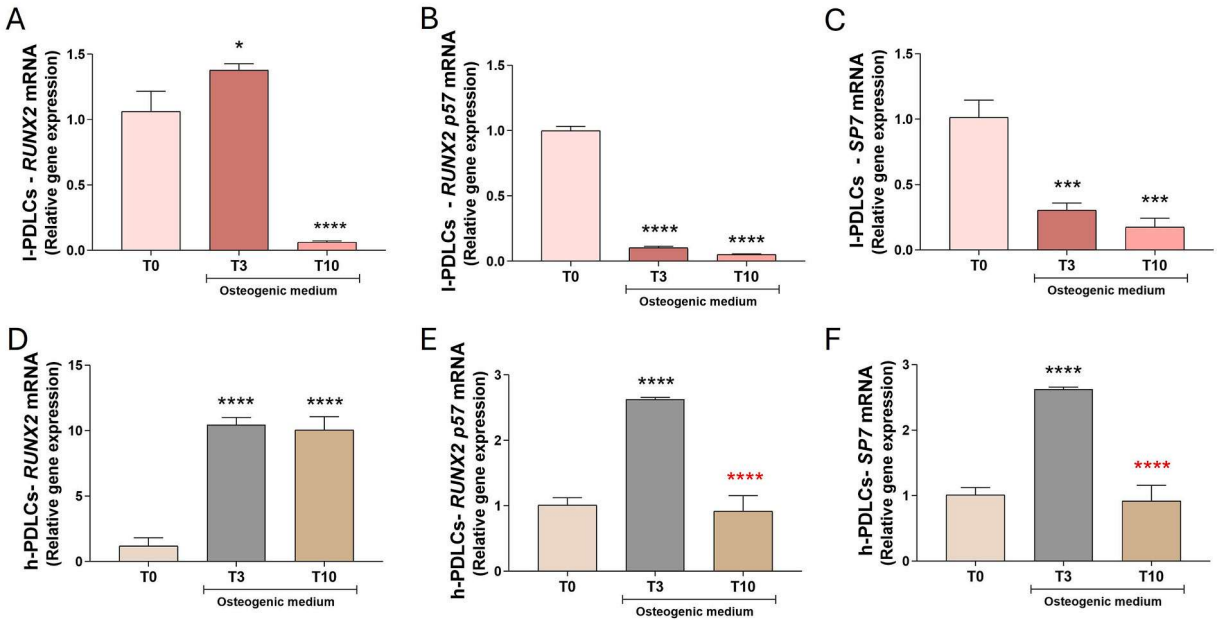

Fig. 3. Transcriptional profiles of *RUNX2*, *RUNX2/P57* and *SP7* differ between PDLCs with high and low osteogenic potential during osteogenic induction. Graphics show the qPCR results of *RUNX2* (A, D), *RUNX2/P57* (B, E) and *SP7* (C, F) in l-PDLCs and h-PDLCs at basal levels (T0) and after 3 and 10 days of osteogenic stimulus (T3 and T10). The relative gene expression levels were determined by using the cycle threshold (Ct) method, and correspond to mRNA levels ratio normalized to *ACTIN-B* levels. The results are represented as mean ± SD of three independent experiments. Statistical diferences were performed by ANOVA one way followed by Tukey test. *$p \leq 0.05$, ***$p \leq 0.001$ and ****$p \leq 0.0001$ compared to T0; ****$p \leq 0.0001$ compared to T3. h-PDLCs, high osteogenic potential; l-PDLCs, low osteogenic potential.

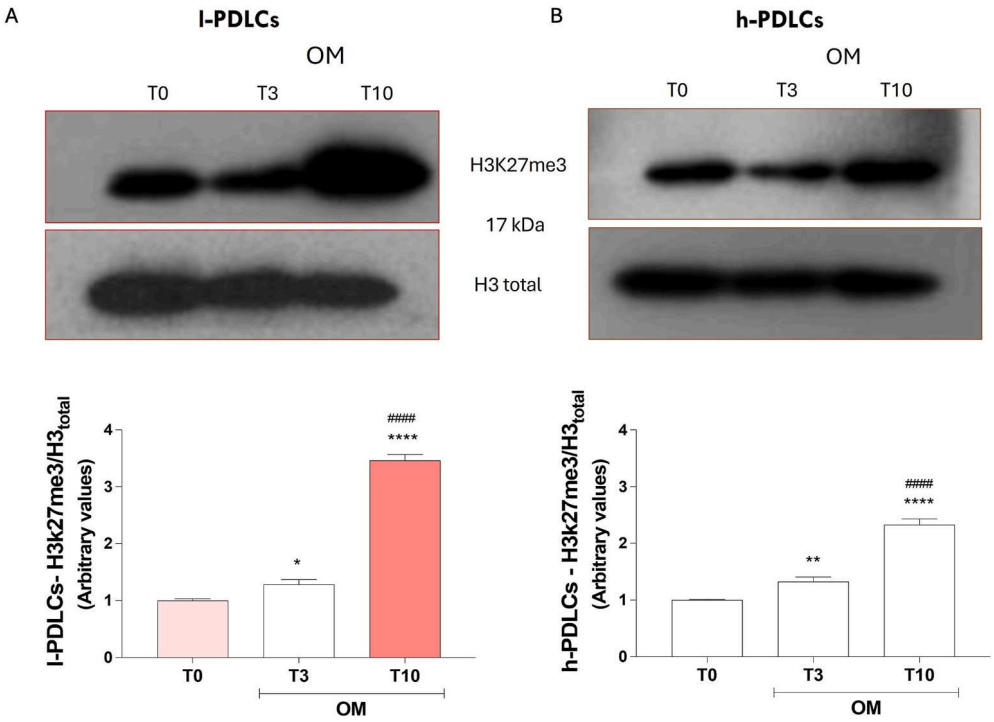

Fig. 4. Global H3K27me3 levels differ between PDLCs with distinct osteogenic phenotypes during osteogenic induction. Immunoblot of whole cell extracts from l-PDLCs (A) and h-PDLCs (B) using antibodies against H3K27me3 and H3 are shown. (C, D) Densitometric analysis of immunoblots were measured using the ImageJ Software normalized to the protein ratio of controls, which were normalized by 1, with H3 as loading control. Statistical diferences were performed by ANOVA one way followed by Tukey test. *p ≤ 0.05, **p ≤ 0.01 and ****p ≤ 0.0001 compared to T0; ####p ≤ 0.0001 compared to T3. h-PDLCs, high osteogenic potential; l-PDLCs, low osteogenic potential.

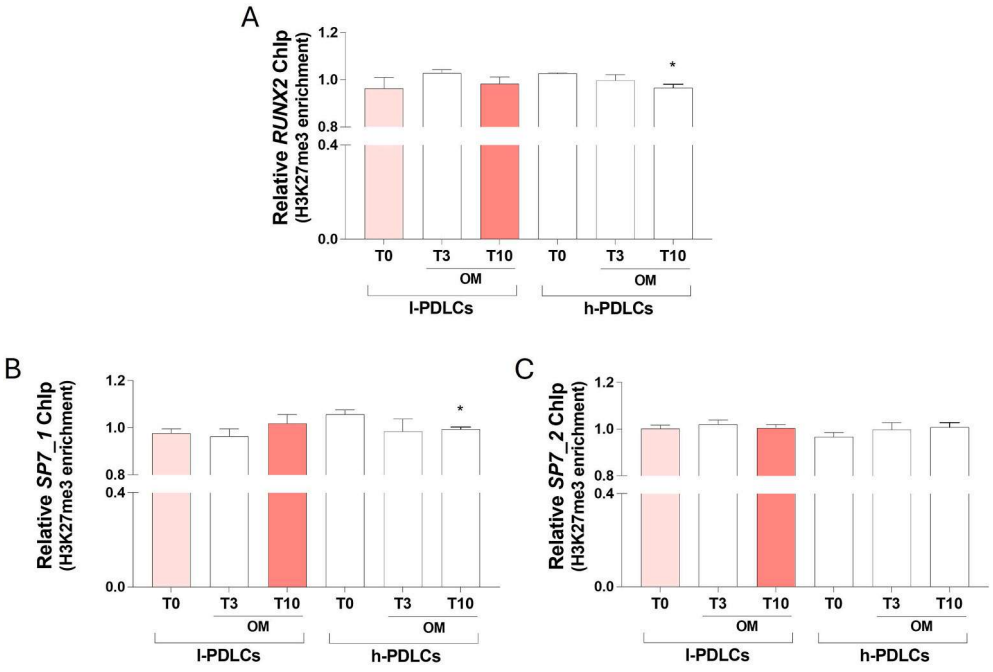

Fig. 5. The promoter-specific regions of *RUNX2* and *SP7* are characterized by distinct patterns of the repressive histone modification mark H3K27me3 in both l-PDLCs and hPDLCs. One region of *RUNX2* (A) and two regions of *SP7* (B, C) upstream to the transcription start site (TSS) of both genes were probed for histone H3K27me3 enrichment with one primer pair each reagion. Primer binding sites location at promoters are −1136 to 1031 for *RUNX2,* 78 to −202 for *SP7_1* and −1445 and −1315 for *SP7_2* (Gopinathan et al., 2023). ChIP-qPCR based histone H3K27me3 (A, B, C) enrichment at those regions above indicated on *RUNX2* and *SP7* promoters, respectively. ChIP-qPCR analyses were independently performed with each primer pair and enrichment values (n = 3) are graphed as mean ± SD. Statistical diferences were performed by ANOVA two way followed by Tukey test and are graphed as mean ± SD. * indicates statistical difference amongst T10 and T0 within the same cell population (p ≤ 0.01). h-PDLCs, high osteogenic potential; l-PDLCs, low osteogenic potential.

osteogenic phenotype of PDLCs, with a focus on how chromatin-based mechanisms influence differentiation potential (Ferreira et al., 2024;

Assis et al., 2022; Ferreira et al., 2023; Ferreira et al., 2024). Here, we show that PDLCs with distinct osteogenic potentials display consistent differences in transcriptional and epigenetic profiles that correlate with the expression of the transcription factors *RUNX2* and *SP7* and the epigenetic regulators EZH2, KDM6B, and H3K27me3.

EZH2 mediates trimethylation of histone H3 at lysine 27 (H3K27me3), a repressive histone mark linked to chromatin condensation and transcriptional silencing. Its role in osteogenic differentiation is context dependent. In this study, h-PDLCs exhibited higher *EZH2* and H3K27me3 levels, coupled with low *RUNX2p57* and *SP7* transcript abundance at baseline. Upon osteogenic induction, *RUNX2*, *RUNX2p57*, and *SP7* transcripts increased, consistent with greater osteogenic commitment. In contrast, l-PDLCs showed *EZH2* transcript levels nearly threefold higher than h-PDLCs at induction onset, with low *RUNX2*, *RUNX2p57*, and *SP7* expression, consistent with reduced commitment. These associations are consistent with previous reports showing that EZH2 suppresses osteogenesis in MSCs by repressing key osteogenic genes, including *RUNX2* and *SP7* (Hemming et al., 2014; Dudakovic et al., 2020; Liu et al., 2022). Conversely, KDM6B, a histone demethylase that specifically removes H3K27me3, was more highly expressed in h-PDLCs, particularly at early differentiation stages consistent with its previously described involvement in osteogenic differentiation by activating transcription of osteogenic genes (Yang et al., 2013; Wu et al., 2017; Gopinathan et al., 2023). The reciprocal regulation between *EZH2* and *KDM6B* observed here supports the concept that the dynamic balance between methylation and demethylation of H3K27 is critical for MSC fate decisions (Yang et al., 2013).

An intriguing observation was the increase in H3K27me3 protein levels despite reduced *EZH2* expression at T10. This could be explained by: (1) a self-reinforcing feedback mechanism whereby H3K27me3 recruits PRC2 to propagate the mark even with limited enzymatic availability (Zhang et al., 2015); (2) the inherent stability of this histone modification (Margueron and Reinberg, 2011); and (3) reduced demethylase activity, as in l-PDLCs, which may lead to H3K27me3 accumulation independently of EZH2 (Laugesen et al., 2019). In this study, *KDM6B* expression decreased in l-PDLCs but increased in h-PDLCs, potentially explaining discrepancies between enzyme expression and histone mark abundance.

A limitation of this work is the absence of protein-level data for EZH2 and KDM6B. RUNX2 is a master transcription factor for osteoblast differentiation. Here, its transcripts displayed a biphasic expression pattern during osteogenic stimulation, with early and sustained upregulation in h-PDLCs, consistent with its role in initiating osteogenic programs and activating downstream targets such as SP7 (Nakashima et al., 2002; Bialek et al., 2004; Komori, 2010; Li et al., 2017).

Differences in *RUNX2p57* and *SP7* expression between PDLC populations suggest fine-tuned regulation of osteogenic transcriptional networks, likely mediated by epigenetic modifications. *SP7* expression is known to be tightly regulated by chromatin remodeling and is sensitive to EZH2 activity (Hojo et al., 2022; Li et al., 2020). Persistent H3K27me3 enrichment at *RUNX2* and *SP7* promoters in l-PDLCs may be associated with reduced transcriptional activation, whereas removal of these marks in h-PDLCs facilitates expression. Similar mechanisms have been described in bone marrow–derived MSCs, where H3K27me3 removal is a prerequisite for efficient osteoblastogenesis (Wei et al., 2011; Dudakovic et al., 2020; Montecino et al., 2021; Gao et al., 2024). Importantly, the present study is based on correlative analyses and does not establish direct causal relationships between EZH2/KDM6B activity, H3K27me3 enrichment and osteogenic differentiation. Functional perturbation studies will be required to directly test the mechanistic contribution of these epigenetic regulators to PDLC osteogenic commitment. Within this context, the strength of the present work lies in the consistency of these correlations across transcriptional, protein, and chromatin-level analyses.

Collectively, these findings show that differences in osteogenic potential among PDLCs correlate with coordinated changes in the expression of *RUNX2* and *SP7* and in epigenetic features involving EZH2, KDM6B, and H3K27me3, supporting epigenetic profiling as a valuable approach to characterize osteogenic heterogeneity in periodontal ligament cells.

CRediT authorship contribution statement

D.C. Andia: Writing – review & editing, Writing – original draft, Visualization, Validation, Supervision, Resources, Project administration, Investigation, Funding acquisition, Conceptualization. **L.F. Oliveira:** Writing – review & editing, Investigation, Formal analysis, Data curation. **G.S. Feltran:** Writing – review & editing, Visualization, Investigation, Formal analysis, Data curation. **A.A.S. Gonçalves:** Writing – review & editing, Methodology, Investigation, Formal analysis. **W.F. Zambuzzi:** Writing – review & editing, Writing – original draft, Supervision, Resources, Project administration, Conceptualization. **R.A. da Silva:** Writing – review & editing, Writing – original draft, Visualization, Validation, Supervision, Resources, Project administration, Conceptualization.

Data availability statement

Data supporting these findings are available upon request or through the Paulista University Repository at https://repositorio.unip.br/wp-admin/admin.php?page=tainacan_admin#/collections.

Funding

This work was supported by São Paulo Research Foundation – FAPESP (grant number: 2022/04770-4) and Higher Education Personnel Improvement Coordination (Brazil) – CAPES (financing code: 001).

Declaration of conflicting interests

The authors declared no potential conflicts of interest with respect to the research, authorship, and/or publication of this article.

Appendix

Table 1 Primer sequences and qPCR and ChIP qPCR cycle conditions.

Gene	Primers qPCR	5' - 3' sequence	Reaction conditions	bp
RUNX2	Forward	CCGTCCATCCACTCTACCCA	95 °C—15 s; 57 °C—30 s; 72 °C—30 s	289
	Reverse	ATGAAATGCTTGGGAACTGC		
RUNX2p57	Forward	GGTTAATCTCCGCAGGTCCA	95 °C—15 s; 55 °C—30 s; 72 °C—30 s	345
	Reverse	GTCACTGTGCTGAAGGGACT		
SP7	Forward	CCAGGCAACACTCCTACTCC	95 °C—15 s; 59 °C—30 s; 72 °C—30 s	473

(*continued on next page*)

(*continued*)

Gene	Primers qPCR	5' - 3' sequence	Reaction conditions	bp
β-ACTIN	Reverse Forward Reverse	GCCTTGCCATACACCT TGC GCACAGAGCCTCGCCTT GTTGTCGAC GACGAG CG	95 °C—10 s; 58 °C—30 s; 72 °C—30 s	253

Gene	Primers ChIP qPCR	5'- 3' sequence	Reaction conditions
RUNX2	Forward Reverse	ACCCAAACCCTGCAAAATCT TTCTTGAGCCTCTGTGCTGA	95 °C—10 s; 57 °C—20 s; 72 °C—30 s
SP7_1	Forward Reverse	TGTGTGTCCGTCTGTGTTCA GAGAGACTGGAACGCACTGA	95 °C—10 s; 57 °C—20 s; 72 °C—30 s
SP7_2	Forward Reverse	TCTATCAGCCACCTGGTTCC CAGCAGGTAGGCACCAATTT	95 °C—10 s; 57 °C—20 s; 72 °C—30 s

References

Adolpho, L.F., Lopes, H.B., Freitas, G.P., Weffort, D., Totoli, G.G.C., Barbosa, A.C.L., Assis, R.I.F., Ruiz, K.G.S., Andia, D.C., Rosa, A., 2022. Human periodontal ligament stem cells with distinct osteogenic potential induce bone formation in rat calvaria defects. Regen. Med. 17 (6), 341–353. https://doi.org/10.2217/rme-2021-0178.

Aguilar, R., Bustos, F.J., Saez, M., Rojas, A., Allende, M.L., van Wijnen, A.J., van Zundert, B., Montecino, M., 2016. Polycomb PRC2 complex mediates epigenetic silencing of a critical osteogenic master regulator in the hippocampus. Biochim. Biophys. Acta 1859 (8), 1043–1055. https://doi.org/10.1016/j.bbagrm.2016.05.009.

Assis, R.I.F., Schmidt, A.G., Racca, F., da Silva, R.A., Zambuzzi, W.F., Silvério, K.G., Nociti Jr., F.H., Pecorari, V.G., Wiench, M., Andia, D.C., 2021. DNMT1 inhibitor restores RUNX2 expression and mineralization in periodontal ligament cells. DNA Cell Biol. 40 (5), 662–674. https://doi.org/10.1089/dna.2020.6239.

Assis, R.I.F., Racca, F., Ferreira, R.S., Ruiz, K.G.S., da Silva, R.A., Clokie, S.J.H., Wiench, M., Andia, D.C., 2022. Osteogenic commitment of human periodontal ligament cells is predetermined by methylation, chromatin accessibility and expression of key transcription factors. Cells 11 (7), 1126. https://doi.org/10.3390/cells11071126.

Bialek, P., Kern, B., Yang, X., Schrock, M., Sosic, D., Hong, N., Wu, H., Yu, K., Ornitz, D. M., Olson, E.N., et al., 2004. A twist code determines the onset of osteoblast differentiation. Dev. Cell 6 (3), 423–435. https://doi.org/10.1016/s1534-5807(04)00058-9.

Cabaña-Muñoz, M.E., Pelaz Fernández, M.J., Parmigiani-Cabaña, J.M., Parmigiani-Izquierdo, J.M., Merino, J.J., 2023. Adult mesenchymal stem cells from oral cavity and surrounding areas: types and biomedical applications. Pharmaceutics 15 (8), 2109. https://doi.org/10.3390/pharmaceutics15082109.

da Silva, R.A., da, C., Fernandes, C.J., Feltran, G.D.S., Gomes, A.M., Andrade, A.F.C., Andia, D.C., Peppelenbosch, M.P., Zambuzzi, W.F., 2019. Laminar shear stress-provoked cytoskeletal changes are mediated by epigenetic reprogramming of TIMP1 in human primary smooth muscle cells. J. Cell. Physiol. 234 (5), 6382–6396. https://doi.org/10.1002/jcp.27374.

Ducy, P., Zhang, R., Geoffroy, V., Ridall, A.L., Karsenty, G., 1997. Osf2/Cbfa1: a transcriptional activator of osteoblast differentiation. Cell 89 (5), 747–754. https://doi.org/10.1016/s0092-8674(00)80257-3.

Dudakovic, A., Samsonraj, R.M., Paradise, C.R., Galeano-Garces, C., Mol, M.O., Galeano-Garces, D., Zan, P., Galvan, M.L., Hevesi, M., Pichurin, O., et al., 2020. Inhibition of the epigenetic suppressor EZH2 primes osteogenic differentiation mediated by BMP2. J. Biol. Chem. 295 (23), 7877–7893. https://doi.org/10.1074/jbc.RA119.011685.

Ferreira, R.S., Assis, R.I.F., Feltran, G.D.S., do Rosário Palma, I.C., Françoso, B.G., Zambuzzi, W.F., Andia, D.C., da Silva, R.A., 2022. Genome-wide DNA (hydroxy) methylation reveals the individual epigenetic landscape importance on osteogenic phenotype acquisition in periodontal ligament cells. J. Periodontol. 93 (3), 435–448. https://doi.org/10.1002/JPER.21-0218.

Ferreira, R.S., Assis, R.I.F., Racca, F., Bontempi, A.C., da Silva, R.A., Wiench, M., Andia, D.C., 2023. Analyzes in silico indicate the lncRNAs MIR31HG and LINC00939 as possible epigenetic inhibitors of the osteogenic differentiation in PDLCs. Genes 14 (8), 1649. https://doi.org/10.3390/genes14081649.

Ferreira, R.S., da Silva, R.A., Feltran, G.D.S., da Silva, E.P., de Assis, R.I.F., Rovai, E.S., Zambuzzi, W.F., Andia, D.C., 2024. JARID1B represses the osteogenic potential of human periodontal ligament mesenchymal cells. Oral Dis. 30 (6), 3971–3981. https://doi.org/10.1111/odi.14814.

Gao, C.W., Lin, W., Riddle, R.C., Kushwaha, P., Boukas, L., Björnsson, H.T., Hansen, K.D., Fahrner, J.A., 2024. A mouse model of Weaver syndrome displays overgrowth and excess osteogenesis reversible with KDM6A/6B inhibition. JCI Insight 9 (1), e173392. https://doi.org/10.1172/jci.insight.173392.

Gopinathan, G., Kolokythas, A., Luan, X., Diekwisch, T.G.H., 2013. Epigenetic marks define the lineage and differentiation potential of two distinct neural crest-derived intermediate odontogenic progenitor populations. Stem Cell. Dev. 22 (12), 1763–1778. https://doi.org/10.1089/scd.2012.0711.

Gopinathan, G., Luan, X., Diekwisch, T.G.H., 2023. Epigenetic repression of RUNX2 and OSX promoters controls the nonmineralized state of the periodontal ligament. Genes 14 (1), 201. https://doi.org/10.3390/genes14010201.

Hargreaves, K.M., Diogenes, A., Teixeira, F.B., 2013. Treatment options: biological basis of regenerative endodontic procedures. Pediatr. Dent. 35 (2), 129–140.

Hemming, S., Cakouros, D., Isenmann, S., Cooper, L., Menicanin, D., Zannettino, A., Gronthos, S., 2014. EZH2 and KDM6A act as an epigenetic switch to regulate mesenchymal stem cell lineage specification. Stem Cell. 32 (3), 802–815. https://doi.org/10.1002/stem.1573.

Hojo, H., Saito, T., He, X., Guo, Q., Onodera, S., Azuma, T., Koebis, M., Nakao, K., Aiba, A., Seki, M., et al., 2022. Runx2 regulates chromatin accessibility to direct the osteoblast program at neonatal stages. Cell Rep. 40 (10), 111315. https://doi.org/10.1016/j.celrep.2022.111315.

Komori, T., 2010. Regulation of osteoblast differentiation by Runx2. Adv. Exp. Med. Biol. 658, 43–49. https://doi.org/10.1007/978-1-4419-1050-9.

Lapunzina, P., Aglan, M., Temtamy, S., Caparrós-Martín, J.A., Valencia, M., Letón, R., Martínez-Glez, V., Elhossini, R., Amr, K., Vilaboa, N., et al., 2010. Identification of a frameshift mutation in Osterix in a patient with recessive osteogenesis imperfecta. Am. J. Hum. Genet. 87 (1), 110–114. https://doi.org/10.1016/j.ajhg.2010.05.016.

Laugesen, A., Højfeldt, J.W., Helin, K., 2019. Molecular mechanisms directing PRC2 recruitment and H3K27 methylation. Mol. Cell 74 (1), 8–18. https://doi.org/10.1016/j.molcel.2019.03.011.

Li, H., Liefke, R., Jiang, J., Kurland, J.V., Tian, W., Deng, P., Zhang, W., He, Q., Patel, D. J., Bulyk, M.L., et al., 2017. Polycomb-like proteins link the PRC2 complex to CpG islands. Nature 549 (7671), 287–291. https://doi.org/10.1038/nature23881.

Li, Z., Guo, X., Wu, S., 2020. Epigenetic silencing of KLF2 by long non-coding RNA SNHG1 inhibits periodontal ligament stem cell osteogenesis differentiation. Stem Cell Res. Ther. 11 (1), 435. https://doi.org/10.1186/s13287-020-01953-8.

Liu, Z., Lee, H.L., Suh, J.S., Deng, P., Lee, C.R., Bezouglaia, O., Mirnia, M., Chen, V., Zhou, M., Cui, Z.K., et al., 2022. The ERα/KDM6B regulatory axis modulates osteogenic differentiation in human mesenchymal stem cells. Bone Res. 10 (1), 3. https://doi.org/10.1038/s41413-021-00171-z.

Margueron, R., Reinberg, D., 2011. The Polycomb complex PRC2 and its mark in life. Nature 469 (7330), 343–349. https://doi.org/10.1038/nature09784.

Meyer, M.B., Benkusky, N.A., Pike, J.W., 2014. The RUNX2 cistrome in osteoblasts: characterization, down-regulation following differentiation, and relationship to gene expression. J. Biol. Chem. 289 (23), 16016–16031. https://doi.org/10.1074/jbc.M114.552216.

Montecino, M., Carrasco, M.E., Nardocci, G., 2021. Epigenetic control of osteogenic lineage commitment. Front. Cell Dev. Biol. 8, 611197. https://doi.org/10.3389/fcell.2020.611197.

Mundlos, S., Otto, F., Mundlos, C., Mulliken, J.B., Aylsworth, A.S., Albright, S., Lindhout, D., Cole, W.G., Henn, W., Knoll, J.H., et al., 1997. Mutations involving the transcription factor CBFA1 cause cleidocranial dysplasia. Cell 89 (5), 773–779. https://doi.org/10.1016/s0092-8674(00)80260-3.

Nakashima, K., Zhou, X., Kunkel, G., Zhang, Z., Deng, J.M., Behringer, R.R., de Crombrugghe, B., 2002. The novel zinc finger-containing transcription factor osterix is required for osteoblast differentiation and bone formation. Cell 108 (1), 17–29. https://doi.org/10.1016/s0092-8674(01)00622-5.

Rojas, A., Aguilar, R., Henriquez, B., Lian, J.B., Stein, J.L., Stein, G.S., van Wijnen, A.J., van Zundert, B., Allende, M.L., Montecino, M., 2015. Epigenetic control of the bone-master Runx2 gene during osteoblast-lineage commitment by the histone demethylase JARID1B/KDM5B. J. Biol. Chem. 290 (47), 28329–28342. https://doi.org/10.1074/jbc.M115.657825.

Tai, P.W.L., Wu, H., Gordon, J.A.R., Whitfield, T.W., Barutcu, A.R., van Wijnen, A.J., Lian, J.B., Stein, G.S., Stein, J.L., 2014. Epigenetic landscape during osteoblastogenesis defines a differentiation-dependent Runx2 promoter region. Gene 550 (1), 1–9. https://doi.org/10.1016/j.gene.2014.05.044.

Voigt, P., Tee, W.W., Reinberg, D., 2013. A double take on bivalent promoters. Genes Dev. 27 (12), 1318–1338. https://doi.org/10.1101/gad.219626.113.

Wei, Y., Gañán-Gómez, I., Salazar-Dimicoli, S., McCay, S.L., Garcia-Manero, G., 2011. Histone methylation in myelodysplastic syndromes. Epigenomics 3 (2), 193–205. https://doi.org/10.2217/epi.11.9.

Wu, H., Whitfield, T.W., Gordon, J.A.R., Dobson, J.R., Tai, P.W.L., van Wijnen, A.J., Stein, J.L., Stein, G.S., Lian, J.B., 2014. Genomic occupancy of Runx2 with global expression profiling identifies a novel dimension to control of osteoblastogenesis. Genome Biol. 15 (3), R52. https://doi.org/10.1186/gb-2014-15-3-r52.

Wu, H., Gordon, J.A.R., Whitfield, T.W., Tai, P.W.L., van Wijnen, A.J., Stein, J.L., Stein, G.S., Lian, J.B., 2017. Chromatin dynamics regulate mesenchymal stem cell

lineage specification and differentiation to osteogenesis. Biochim Biophys Acta Gene Regul Mech 1860 (4), 438–449. https://doi.org/10.1016/j.bbagrm.2017.01.003.
Yang, D., Okamura, H., Nakashima, Y., Haneji, T., 2013. Histone demethylase Jmjd3 regulates osteoblast differentiation via transcription factors Runx2 and osterix. J. Biol. Chem. 288 (47), 33530–33541. https://doi.org/10.1074/jbc.M113.497040.
Yeasmin, S., Ceccarelli, J., Vigen, M., Carrion, B., Putnam, A.J., Tarle, S.A., Kaigler, D., 2014. Stem cells derived from tooth periodontal ligament enhance functional angiogenesis by endothelial cells. Tissue Eng. 20 (7–8), 1188–1196. https://doi.org/10.1089/ten.TEA.2013.0512.
Yu, S., Jiang, Y., Galson, D.L., Luo, M., Lai, Y., Lu, Y., Ouyang, H.J., Zhang, J., Xiao, G., 2008. General transcription factor IIA-gamma increases osteoblast-specific osteocalcin gene expression via activating transcription factor 4 and runt-related transcription factor 2. J. Biol. Chem. 283 (9), 5542–5553. https://doi.org/10.1074/jbc.M705653200.
Zhang, F., Xu, L., Xu, L., Xu, Q., Karsenty, G., Chen, C.D., 2015. Histone demethylase JMJD3 is required for osteoblast differentiation in mice. Sci. Rep. 5, 13418. https://doi.org/10.1038/srep13418.
Zhou, X., Zhang, Z., Feng, J.Q., Dusevich, V.M., Sinha, K., Zhang, H., Darnay, B.G., de Crombrugghe, B., 2010. Multiple functions of Osterix are required for bone growth and homeostasis in postnatal mice. Proc. Natl. Acad. Sci. U. S. A. 107 (29), 12919–12924. https://doi.org/10.1073/pnas.0912855107.